SUPPLEMENTARY MATERIAL

Contactless pick-and-place of millimetric objects using inverted near-field acoustic levitation

Marco A. B. Andrade[1], Tiago S. Ramos[2], Julio C. Adamowski[3], and Asier Marzo[4]

AFFILIATIONS

[1]Instituto de Física, Universidade de São Paulo, São Paulo 05508-090, Brazil
[2]Physics Department, University of Massachusetts, Amherst, MA 01003, USA
[3]Escola Politécnica, Universidade de São Paulo, São Paulo 05508-030, Brazil
[4]UpnaLab, Universidad Pública de Navarra, Pamplona 31006, Navarra, Spain

S1. Design and fabrication of the Langevin transducer

The contactless manipulation of SMD components is performed with a bolt-clamped Langevin type transducer, which was specially designed for this task. The Langevin type transducer consists of a sandwich structure and a mechanical amplifier, as illustrated in Fig. S1. The sandwich structure is formed by two piezoelectric rings, which are compressed between two aluminum blocks by a central bolt. The mechanical amplifier basically consists of two aluminum cylindrical blocks of different diameters. When a sinusoidal electric signal is applied at the electrodes of the piezoelectric rings, the sandwich structure vibrates as a half-wavelength resonator. The axial vibration generated by the sandwich structure is amplified by the mechanical amplifier, allowing high displacement amplitudes at the transducer tip. The mechanical amplifier also works as a half-wavelength resonator. The axial displacement profile along the transducer is shown in Fig. S1.

The transducer was designed to operate at 21 kHz. This frequency was chosen because it is above the range of human hearing and it meets the condition for obtaining an attractive force on the target object (i.e. $R/\lambda < 0.38$). The transducer is simulated and designed using the Finite Element Method (FEM) software COMSOL Multiphysics. The

transducer design is carried out in two steps. First, the sandwich structure is simulated using an axisymmetric FEM model and its geometric parameters are manually adjusted until the sandwich structure resonates at the desired frequency (i.e. 21 kHz). Then another model is used to simulate and design the mechanical amplifier.

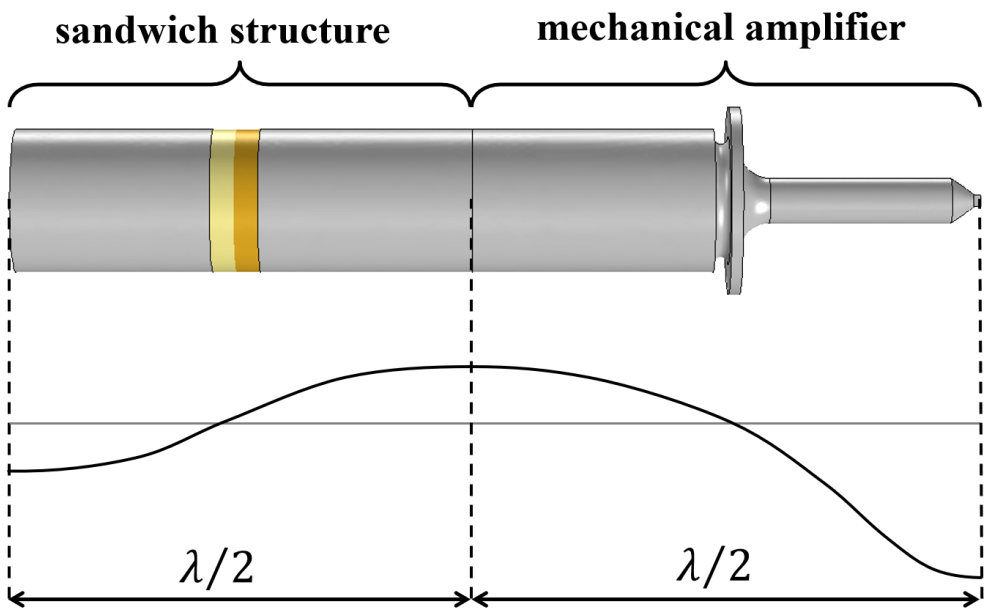

FIG. S1. Langevin type transducer consisting of two main parts: a sandwich structure and a mechanical amplifier. Each part operates as a half-wavelength resonator, as illustrated in the axial displacement profile.

The FEM model used for designing the sandwich structure is shown in Fig. S2. The sandwich structure consists of two piezoelectric rings made of Lead Titanate Zirconate (PZT-4) of 38.1 mm external diameter, 12.7 mm internal diameter and 6.35 mm thickness, which are compressed between two aluminum cylindrical blocks by a M10 allen steel bolt. The sandwich structure is illustrated in Fig. S2(a) and its axisymmetric FEM model with the geometric parameters is shown in Fig. S2(b). The aluminum blocks, the steel bolt and the washer were modeled using linear elastic solids elements whereas the piezoelectric rings were modeled using piezoelectric elements. The material properties used in the FEM simulations are presented in Table S1. In the material properties of PZT-4, ρ is the density, C_{ij}^{E} are the stiffness constants at constant electric field, e_{ij} are the piezoelectric constants, and $\varepsilon_{ij}^{S}/\varepsilon_0$ are the dielectric constants, where ε_0 = 8.85 x 10^{-12} F/m is the permittivity of free space. For the aluminum and steel parts, E is the Young's modulus and ν is the Poisson's ratio.

As a starting point, the total length (L) was estimated by approximating the sandwich structure by an aluminum cylindrical bar with a diameter much smaller than its length. For the bar vibrating in its first extensional mode, the total length L is given by:

$$L = \frac{1}{2f}\sqrt{\frac{E}{\rho}}, \tag{S1}$$

where f = 21 kHz is the desired frequency, E = 7 x 10^{10} N/m^2 is the aluminum Young's Modulus and ρ = 2700 kg/m^3 is the aluminum density. Then, by carrying out FEM simulations in the frequency domain, the geometric parameters of Fig. S2(b) were adjusted until the resonance frequency matched the desired frequency of 21 kHz. The final geometric parameters of the sandwich structure after this adjustment process are presented in Table S2. The simulated vibration of the sandwich structure at 21 kHz is shown in Fig. S2(c).

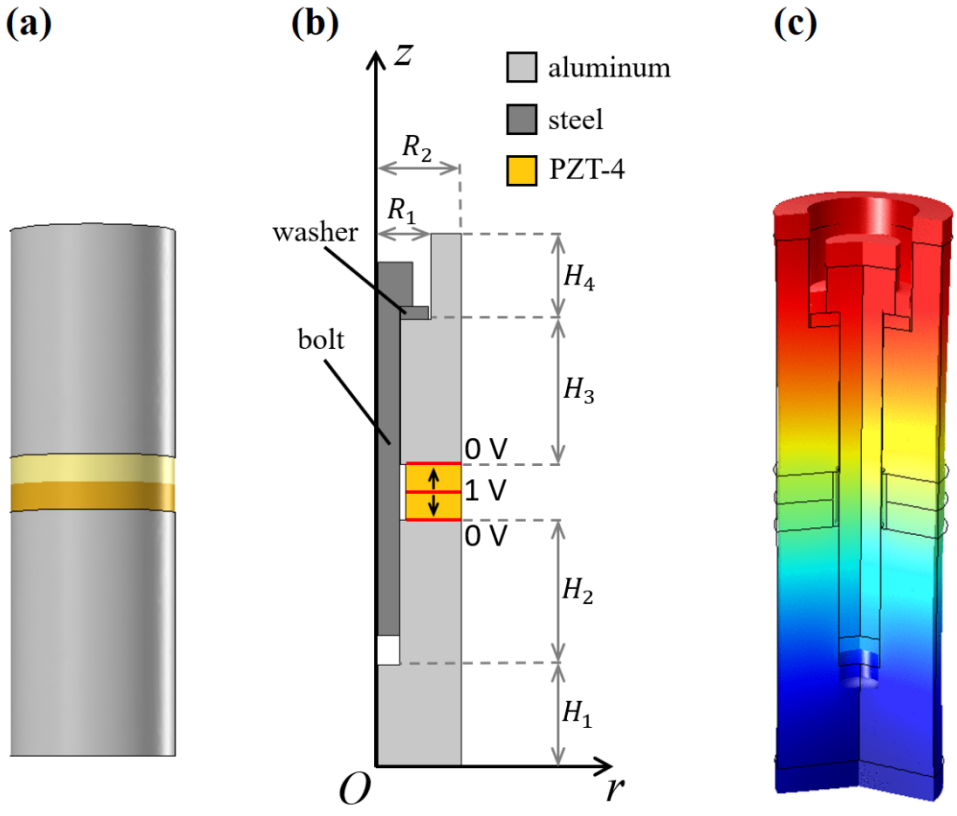

FIG. S2. Simulation and design of the sandwich structure consisting of two piezoelectric rings and two cylindrical blocks. (a) Illustration of the bolt-clamped sandwich structure. (b) Axisymmetric FEM model with its geometrical parameters. (c) Simulated vibration of the sandwich structure at 21 kHz.

TABLE S1. Material properties.

PZT-4	
C_{11}^E (10^{10} N/m^2)	13.90
C_{12}^E (10^{10} N/m^2)	7.78
C_{13}^E (10^{10} N/m^2)	7.43
C_{33}^E (10^{10} N/m^2)	11.54
C_{44}^E (10^{10} N/m^2)	2.56
e_{31} (C/m^2)	-5.20
e_{33} (C/m^2)	15.08
e_{15} (C/m^2)	12.72
$\varepsilon_{11}^S/\varepsilon_0$	762.5
$\varepsilon_{33}^S/\varepsilon_0$	663.2
ρ (kg/m^3)	7500
Aluminum	
E (10^{10} N/m^2)	7.0
ν	0.33
ρ (kg/m^3)	2700
Steel	
E (10^{10} N/m^2)	20
ν	0.33
ρ (kg/m^3)	7850

The mechanical amplifier of the transducer is simulated and designed by carrying out 3D simulations in COMSOL. The FEM model of the mechanical amplifier is shown in Fig. S3(a). The transducer has a rectangular tip with the same lateral dimensions as the SMD resistor (1.6 mm x 3.2 mm). By conducting an Eigenfrequency analysis in COMSOL, the geometric parameters of the mechanical amplifier are adjusted until it resonates at the desired frequency. In this adjustment process, the parameters H_5 and H_7 were carefully adjusted in order to make the amplifier resonate at 21 kHz while reducing the mechanical vibration at the supporting flange located at the middle of the mechanical amplifier. The final geometric parameters after this adjustment process is presented in Table S2. The simulated vibration of the mechanical amplifier at 21 kHz is shown in Fig. S3(b). As shown in this figure, the mechanical amplifier has a low axial displacement on the top and a high displacement amplitude at the transducer tip.

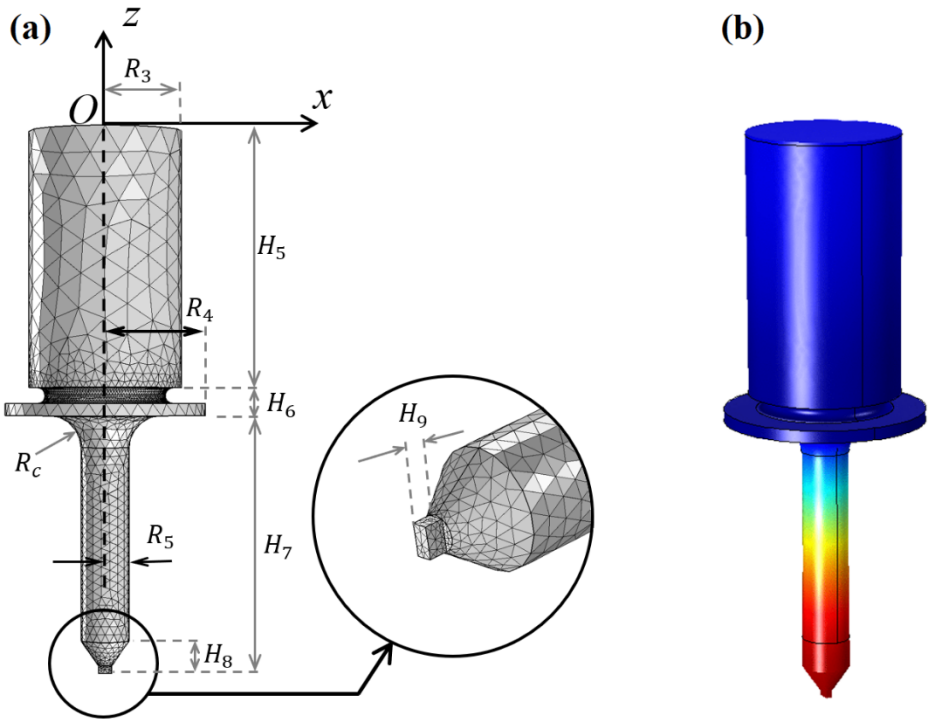

FIG. S3. Simulation and design of the mechanical amplifier. (a) 3D FEM model of the mechanical amplifier. (b) Simulated vibration at 21 kHz.

TABLE S2. Transducer geometric parameters.

Sandwich structure	
H_1	23.5 mm
H_2	33.0 mm
H_3	33.0 mm
H_4	19.5 mm
R_1	12.0 mm
R_2	19.05 mm
Mechanical amplifier	
H_5	64.0 mm
H_6	7.0 mm
H_7	64.3 mm
H_8	8.0 mm
H_9	2.0 mm
R_3	19.05 mm
R_4	25.0 mm
R_5	6.0 mm
R_c	8.0 mm

After designing the sandwich structure and the mechanical amplifier separately, both parts are coupled together and the whole transducer is simulated. The simulated vibration of the transducer at 21 kHz is shown in Fig. S4(a). As shown in Fig. S4(a), when a voltage amplitude of 1 V is applied at the electrodes of the piezoelectric ceramics, the transducer vibrates, generating a large displacement amplitude on the transducer tip.

Using the geometric parameters of Table S2, the parts were machined and the transducer was assembled. To assemble the transducer, a torque wrench was used to apply a torque of 50 Nm to the clamping bolt. A picture of the assembled transducer is shown in Fig. S4(b).

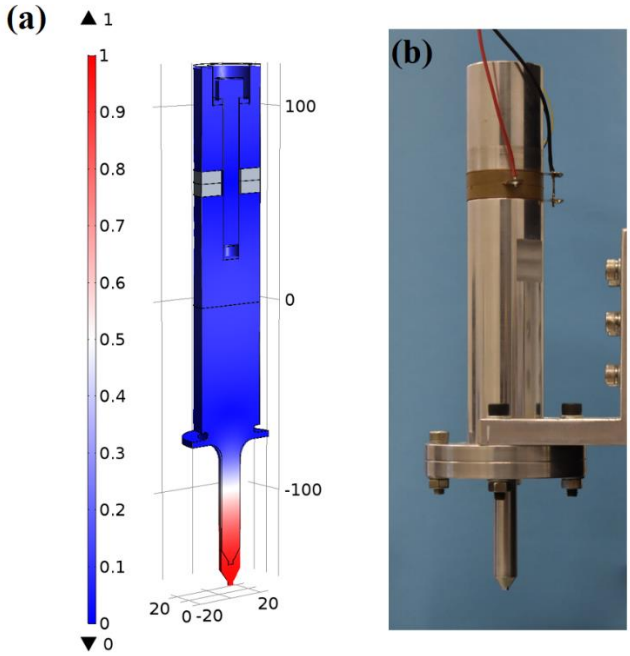

FIG. S4. Langevin type transducer designed for the contactless pick-and-place of SMD components. (a) Simulated vibration at 21 kHz. (b) Picture of the transducer.

S2. Computational Fluid Dynamics (CFD) model

The CFD simulations of the inverted near-field acoustic levitation device were carried out using the Fluid-Structure Interaction (FSI) interface of COMSOL Multiphysics. The axisymmetric CFD model is shown in Fig. S5. An Arbitrary Lagrangian-Eulerian (ALE) formulation was used to model the displacement of the transducer surface located at a mean distance H above the object surface. The object surface ($z = 0$, $0 \leq r \leq 1.27$ mm) was modeled as a rigid wall ($\mathbf{u} = 0$) and the transducer surface was modeled by assuming that its vertical velocity is given by:

$$u_z(t) = A\omega sin(\omega t) step(t), \tag{S3}$$

where A = 10 μm is the displacement amplitude, $\omega = 2\pi f$ is the angular frequency, where f = 21 kHz, and the step function $step(t)$ changes from 0 to 1 in approximately 100 μs.

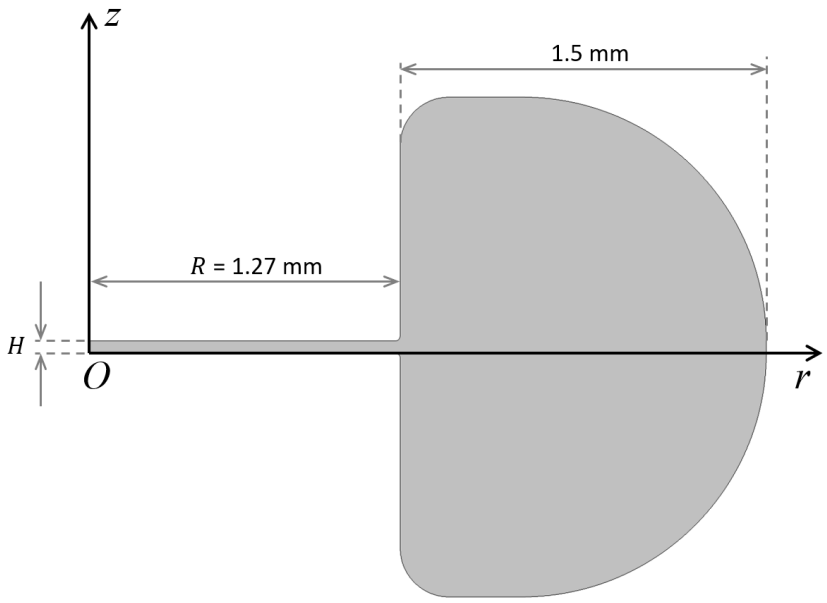

FIG. S5. Computational Fluid Dynamics (CFD) model of the inverted near field acoustic levitation device.

The air medium is modeled using an adiabatic equation of state given by

$$\rho = \rho_0 \left[\frac{p+p_0}{p_0}\right]^{1/\gamma}, \tag{S2}$$

where ρ_0 = 1.2 kg/m^3 is the density of the unperturbed medium, p_0 = 1.01 x 10^5 Pa is the atmospheric pressure and γ = 1.4 is the ratio of specific heats. In addition, it was considered an air dynamic viscosity of 1. 81 x 10^{-5} Pa.s. The simulations were carried out with H varying from 20 μm to 200 μm. For each simulation, the time varied between t = 0 to t = 500 μs.

The CFD simulations simulated the pressure and velocity fields in the air domain as a function of time. A typical simulation result is presented in Fig. S6, which shows the velocity [Figs. S6(a) and S6(b)] and pressure [Fig. S6(c)] fields at t = 408 μs in a simulation with H = 50 μm. To obtain the force on the object, the simulated stress tensor was integrated over the object surface to find the vertical force on the object over time [Fig. S6(d)]. As we can see, although the transducer vibrates sinusoidally, the nonlinearity

of the Navier-Stokes equations causes a non-sinusoidal force on the object surface, whose time-average is nonzero. To find the force on the object, we calculate the time-average force along four periods of the force curve shown in Fig. S6(d). For this particular case, the average vertical force is -11.9 x 10^{-5} N, which corresponds to an attractive force on the object.

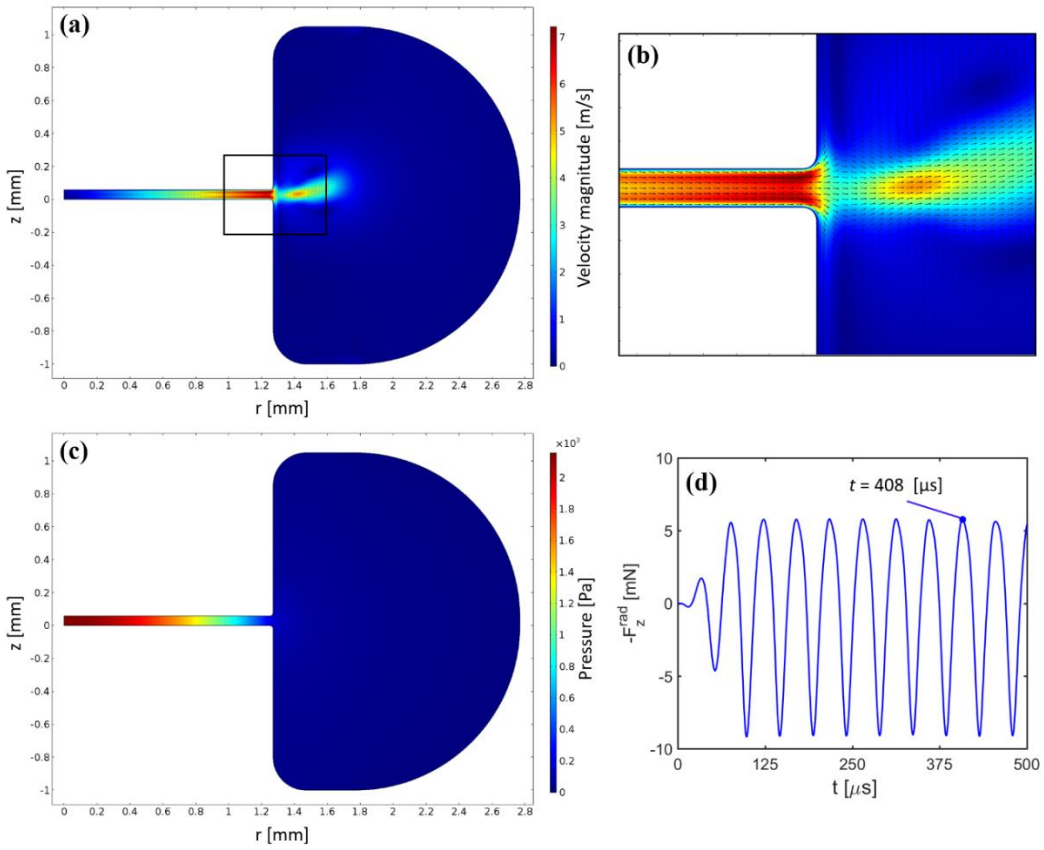

FIG. S6. Results obtained with CFD model for H = 50 µm. (a) Velocity field at t = 408 µs. (b) Zoom-in of the velocity field shown in (a). (c) Pressure field at t = 408 µs. (d) Vertical force on the object over time.

S3. Qualitative matching of experimental and simulated vertical forces

As shown in Fig. S7, there is a good qualitative agreement between the experimental and the simulated vertical force acting on an object. The differences between the numerical and experimental results may be caused by two main factors. On the one hand, the experimental force was measured on a rectangular object, whereas the axisymmetric CFD simulation employed a circular object of radius R = 1.27 mm due to the impossibility of executing a full 3D simulation. On the other hand, the accuracy of the experimental distance measurement was ±10 µm.

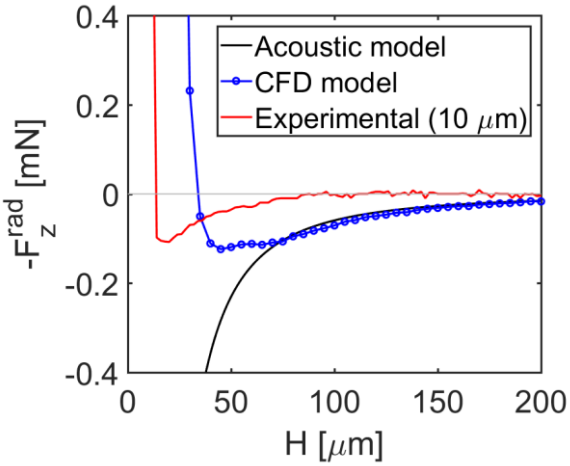

FIG. S7. Time-averaged vertical force exerted on the object as a function of the separation H obtained with the CFD model, the acoustic model and experimental measurements. The experimental results were measured on a SMD component with lateral dimensions of 1.6 mm x 3.2 mm. The results obtained with the acoustic model and the CFD model assumed a circular object of equivalent area (radius R = 1.27 mm).

S4. Effect of air viscosity on the transition from attractive to repulsive forces

We have conducted multiple CFD simulations to investigate the influence of air viscosity on the transition from repulsive to attractive forces. As we can observe in Fig. S8, the value of H (separation between the radiating tip and the object) at which the transition occurs increases with the air dynamic viscosity η. We present in Table S2 the comparison between the viscous penetration depth $\delta = \sqrt{2\eta/\rho_0\omega}$ and the values of H at which the transitions occurred.

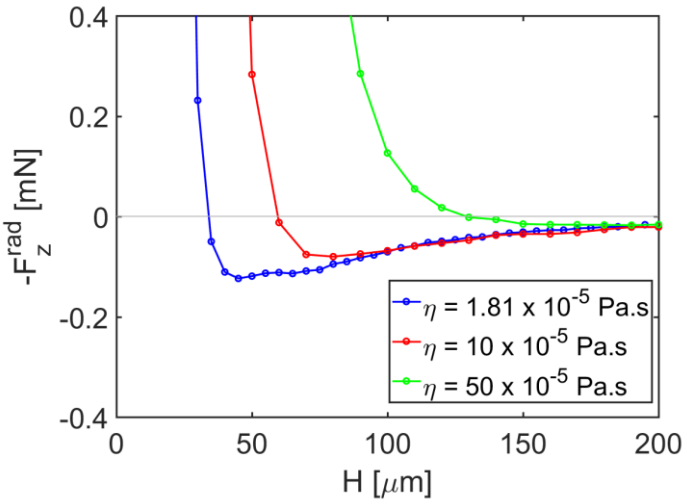

FIG. S8. Simulated vertical force exerted on a circular object of radius R = 1.27 mm for a transducer displacement amplitude of 10 μm, and different values of air dynamic viscosity η.

TABLE S2. Comparison between the viscous penetration depth δ and H (distance of force transition) for different air viscosities η.

η	H (transition)	δ
1.81 x 10^{-5} Pa.s	34 µs	15 µs
10 x 10^{-5} Pa.s	60 µs	35 µs
50 x 10^{-5} Pa.s	130 µs	79 µs

S5. Trapping of a non-flat object

Fig. S9 shows the trapping of an expanded polystyrene sphere of 7 mm in diameter. The sphere is levitated below the transducer without touching the vibrating tip.

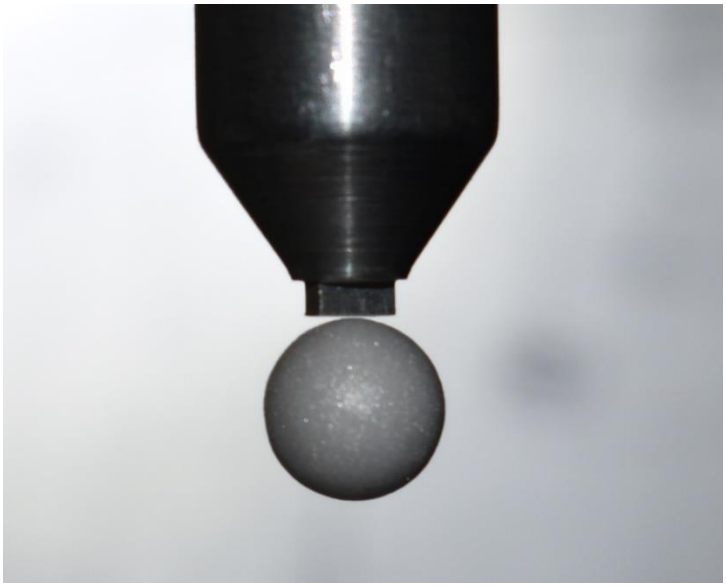

FIG. S9. Non-contact trapping of an expanded polystyrene sphere of 7 mm in diameter.